PAN

Opto-Electronics Review

Application of the Tikhonov and the modified Twomey methods to calculate narrow microparticle size distributions by the laser diffraction technique

Andrzej Pawlata[*], Bartosz Bartosewicz

Institute of Optoelectronics, Military University of Technology, gen. Sylwestra Kaliskiego 2, 00-908 Warsaw, Poland

Article info	Abstract
	New ways of calculating narrow microparticle size distributions based on using the Tikhonov and the modified Twomey methods for the laser diffraction technique are presented. These allow to have reduced the broadening (over-smoothing) of the result occurring in these methods for narrow distributions both singular and their sum. The calculated singular distributions and their distribution sum were then approximated by a Gaussian function and a bimodal Gaussian function, respectively, using the Levenberg-Marquardt method. The angular distribution of scattering power was measured for polystyrene particles with radii of 0.676 µm and 1.573 µm, and for their sum. The tests were carried out for linearly polarized He-Ne laser light scattered by a dilute aqueous suspension of these particles. The results obtained were compared with those obtained with the nanoDS instrument (CILAS). It turned out that using the way based on the Twomey method, the parameters of the narrow distribution sought could be determined quite well.

1.   Introduction

Laser diffraction is a widely used technique for determining particle size distribution distinguished by its large measurement range, fast and easy measurement, and good repeatability. It is based on a direct measurement of the angular power distribution of scattered light resulting from the passage of a laser beam through a set of test particles. By making appropriate simplifying assumptions for the phenomenon of light scattering in a particle system, we can formulate a simple physical measurement model. It combines the directly measured angular power distribution of the scattered light with a calculated particle size distribution function in the form of the Fredholm integral equation of the first kind. The calculation of the particle size distribution function based on this measurement model is an example of an inverse problem and various computational techniques have been developed for its solving. The Tikhonov method [1, 2] and the modified Twomey method [3, 4] were used to calculate two narrow

particle size distributions (coefficient of variation <5%) and their sum.

Since the solutions obtained were considerably over-smoothed, two new ways of obtaining more correct results for narrow particle distributions were proposed in this work. They are based on the appropriate use of the above methods. The first proposed way is a two-step approach using the Tikhonov method. Here, a solution (using Tikhonov method) for the output equation describing the inverse problem was first calculated. Then, the output equation with the obtained solution was scaled and (also using Tikhonov method) this new scaled output equation was solved. It turns out that such a two-step approach results in a solution with significantly less over-smoothing. The second proposed way uses a modified Twomey method. The Twomey method [5–7] was modified by Igushi and Yoshida [3, 4]. By introducing appropriate weighting functions into the calculation method used by Twomey, they obtained a fast and stable algorithm for solving the inverse problem described by the Fredholm equation of the first kind. For this method, for singular distributions, the fundamental problem is the number of iterations to be taken for calculations to obtain the correct

*Corresponding author at: andrzej.pawlata@wat.edu.pl

distribution (the parameters of the distribution, especially its width, depend on the number of iterations). Since the authors of the modified Twomey method did not provide a criterion for choosing the number of iterations, this paper proposes a criterion to find the optimal number of iterations for singular distributions. In this paper, a way to reduce the broadening of the result occurring for this method for the sum of two narrow distributions was proposed. This can be achieved by appropriately calculating the individual singular distributions, sequentially, on the basis of the initially obtained distribution for their sum.

The particle size distributions calculated by the above ways were approximated by Gaussian and bimodal Gaussian functions, respectively, using the Levenberg-Marquardt method [8, 9]. The results obtained by these means were compared with those obtained with the nanoDS instrument (CILAS).

Since in this work, the particles are placed in water inside a quartz cuvette with a square base, a numerical correction of the scattering angle for the Snell's law of refraction and the foreshortening effect [10] was applied. Also, corresponding relations between the scattering angle and the rotation angle of the photomultiplier (PMT) were found to allow an easy calculation of the kernel function of the Fredholm integral. Applied laser diffraction method measures the volume-equivalent radius of a particle defined as the radius of a sphere with a volume equal to that of the particle.

2. Mathematical model

2.1. Assumptions

The following assumptions have been made in a mathematical model of problem:

- incident light on particles is a monochromatic plane wave, linearly polarized with a wavelength λ (in vacuum),
- tested particles are spherical, homogeneous, isotropic with a known refractive index n_r,
- set of particles under study is placed in a homogeneous, isotropic medium with a known refractive index n_o,
- there is no significant multiple scattering,
- scattering image from a set of particles is the sum of images given by individual particles.

For these assumptions, a model of light scattering from a single particle (Fig. 1) based on Mie [11, 12] theory can be adopted. Thus, a mathematical model for measuring the power of light scattered from a set of particles in the form of an integral Fredholm equation of the first kind can be formulated

$$P_s(\theta) = \int_0^\infty \left[\frac{3}{4\pi r^3} K(\theta, r) \right] n_v(r) dr, \qquad (1)$$

where: $P_s(\theta)$ – the power of light scattered at an angle θ to the direction of incident light from a set of $n_v(r)$ measured by a detector with a solid angle Ω, θ – the angle between the direction of propagation $\bar{k}_0$ of the light wave ($\bar{E}_i$ – the direction of the electric vector) and the direction of scattering $\bar{k}_s$ (Fig. 1), $n_v(r)$ – the density of a particle size
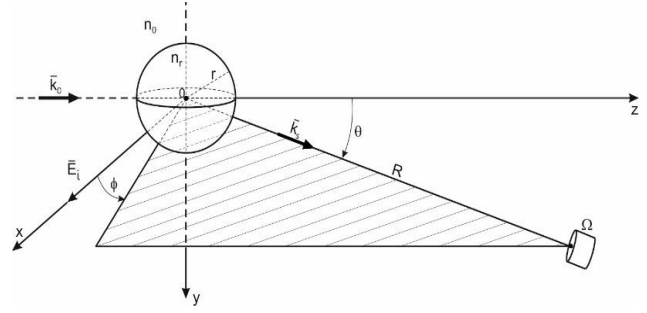

Fig. 1. Single particle scattering geometry.

distribution (radii of spheres) weighted by volume described as

$$n_v(r) = \frac{4\pi r^3}{3} n_n(r),$$

where: $n_n(r)$ – the density of a particle size distribution (radii of spheres) weighted numerically,

$$K(\theta, r) = \frac{I_p}{k_1^2} \iint_\Omega \left[\begin{array}{c} |S_1(\theta, r)|^2 \sin^2(\varphi) \\ + |S_2(\theta, r)|^2 \cos^2(\varphi) \end{array} \right] d\Omega, \quad (2)$$

where φ – the angle between the scattering plane and the direction of the vector $\bar{E}$ of the incident wave, I_p – the intensity of light incident on the particle, $k_1 = \frac{2\pi}{\lambda} n_o$, λ – the wavelength of light in vacuum, r – the radius of the particle and

$$S_1(\theta, r) = \sum_{n=1}^\infty \frac{2n+1}{n(n+1)} [a_n(r)\pi_n(\cos\theta) + b_n(r)\tau_n(\cos\theta)],$$

$$S_2(\theta, r) = \sum_{n=1}^\infty \frac{2n+1}{n(n+1)} [a_n(r)\tau_n(\cos\theta) + b_n(r)\pi_n(\cos\theta)],$$

$$\pi_n(\cos\theta) = \frac{P_n^1(\cos\theta)}{\sin\theta},$$

$$\tau_n(\cos\theta) = \frac{dP_n^1(\cos\theta)}{d\theta},$$

$$a_n(r) = \frac{m\psi_n(mx)\psi_n'(x) - \psi_n(x)\psi_n'(mx)}{m\psi_n(mx)\xi_n'(x) - \xi_n(x)\psi_n'(mx)},$$

$$b_n(r) = \frac{\psi_n(mx)\psi_n'(x) - m\psi_n(x)\psi_n'(mx)}{\psi_n(mx)\xi_n'(x) - m\xi_n(x)\psi_n'(mx)},$$

where: $m = \frac{n_r}{n_o}$, $x = \frac{2\pi r}{\lambda} n_o$ – parameter Mie, P_n^1 – the associated Legendre function of the first kind degree n of order 1, ψ_n, ξ_n – the Riccati-Bessel functions.

The kernel function $K(\theta, r)$ determines the power of light scattered from a particle with the radius r observed on a detector with the solid angle Ω set at the angle (θ, φ) to the direction of the incident light wave $+z$ (Fig. 1). It is independent of the angle φ because the scattering image described by Mie theory for a spherical particle has axial symmetry about the axis z.

2.2. Inverse problem

Determination of the density function of the volume distribution $n_v(r)$ appearing in (1) is an example of an inverse problem, ill-posed in the sense that small changes in the data (due to measurement errors) can cause arbitrarily large changes in the solution. The existence, explicitness, and stability of the solution to this problem can be ensured by using generalized solutions in the sense of the least squares and regularization. The measured signal $P_s(\theta)$ is available only for a finite number of quantities θ contained in the interval of $(\theta_{min}, \theta_{max})$. Because of this, the continuous model has been replaced with an approximate discrete linear model. It is in the form of a system of linear algebraic equations obtained by applying numerical integration by the method of rectangles in the finite interval of (r_{min}, r_{max}) [13]. Evenly and quantitatively equal subintervals were assumed for the arguments θ and r. Then, equation (1) can be written and approximated

$$P_s(\theta_i) = \sum_{j=1}^{n} K1(\theta_i, r_j) n_v(r_j), \qquad (3)$$

where: $P_s(\theta_i)$ – the power of scattered light, measured by the detector for the angle θ_i,

$$K1(\theta_i, r_j) = \frac{3}{4\pi r_j^3} K(\theta_i, r_j)\Delta r, \qquad (4)$$

$n_v(r_j)$ – the sought density of a volume distribution of particles with the radius r_j belonging to class j and

$$\theta_i = \theta_{min} + (i - 0.5)\Delta\theta, \quad \Delta\theta = \frac{\theta_{max} - \theta_{min}}{n},$$
$$i = 1 \ldots n;$$

$$r_j = r_{min} + (j - 0.5)\Delta r, \quad \Delta r = \frac{r_{max} - r_{min}}{n},$$
$$j = 1 \ldots n; \quad n - \text{number of measurements.}$$

The kernel function $K(\theta_i, r_j)$ is calculated from the scattering model Mie (2) for a particle with the radius r_j and the scattering angle θ_i by applying an appropriate algorithm to calculate this scattering [14]. To find the solution $n_v(r)$ for the problem described by the set of (3), the following inverse methods were used:

- linear – Tikhonov regularization [1, 2] (the regularization parameter was selected using the L-curve method [15–17]),
- nonlinear – modified Twomey method [3, 4].

2.3. Measurement geometry

The geometry of the measurement is shown in Fig. 2. The He-Ne laser light propagating along the axis z (in the $+z$ direction) illuminates several particles located on this axis. They are suspended in water inside a quartz cuvette in the shape of a square cuboid with a side square L = 10 mm. The centre of the horizontal cross section of the cuvette lies on the z-axis at a distance z_a from the laser beam waist ($z = 0$), and coincides with the rotation centre of the PMT, located on an arm of length R = 490 mm.

In order to calculate the kernel function $K(\theta_i, r_j)$, both the measurement geometry and the physical phenomena affecting, the measurement result should be taken into account. Therefore, first, the effect of the refraction of scattered light on the back wall of the cuvette on the change in the PMT detection angle θ_i must be taken into account. The effect of scattered light refracted on the cuvette side wall should also be considered, as well as the effect of the transmission of scattered light through back and side wall of the cuvette. The change in the effective solid angle of the PMT with change in a rotation angle (due to refraction of the scattered light) to the magnitude of power measured by the PMT should also be taken into account. Furthermore, it should be noted that influence of these phenomena also depends on the position of the scattering particle inside the cuvette.

For any particle k located at a distance z_k from the beam waist ($z = 0$), and at a distance x_k from the back wall of the
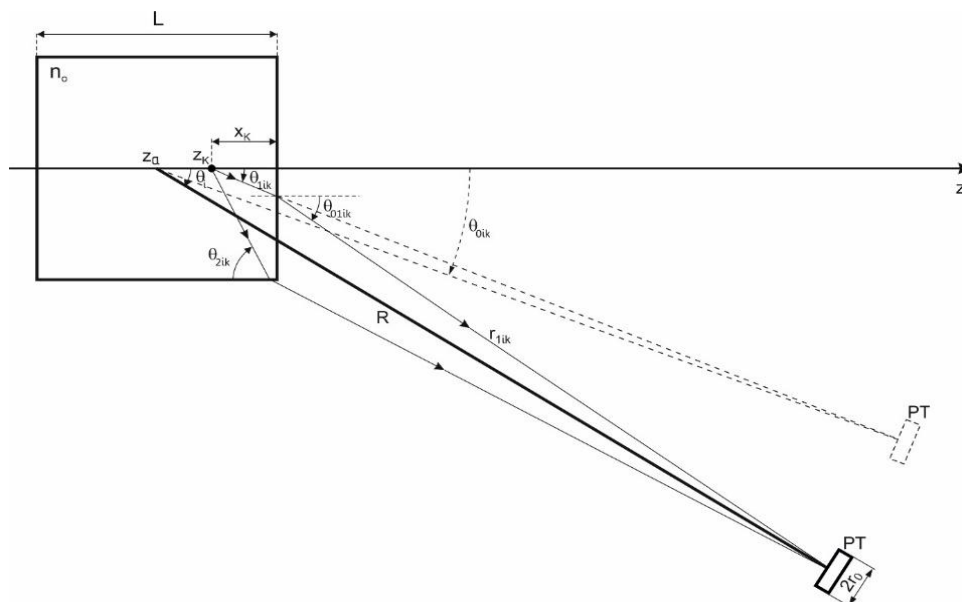

Fig. 2. Measurement geometry.

cuvette, we can derive an equation giving dependence of the scattering angle θ_{1ik} on the detection (rotation) angle of the PMT θ_i in the presence of refraction on the back wall. From Fig. 2, a system of equations [10] can be obtained

$$R \cos \theta_i = \frac{L}{2} + r_{1ik} \cos \theta_{01ik}$$
$$R \sin \theta_i = x_k \tan \theta_{1ik} + r_{1ik} \sin \theta_{01ik} \qquad (5)$$
$$\sin \theta_{01ik} = n_o \sin \theta_{1ik} .$$

Hence, the following relation θ_{1ik} from θ_i is obtained:

$$\left[\left(1 - n_o^2(1-t)\right)\left(tR^2\sin^2\theta_i + x_k^2(1-t)\right) \right.$$
$$\left. - \left(R \cos \theta_i - \frac{L}{2}\right)^2 n_o^2(1-t)t \right]^2 \qquad (6)$$
$$= 4R^2 x_k^2 \sin^2\theta_i \left(1 - n_o^2(1-t)\right)^2 (1-t)t,$$

where $t = \cos^2\theta_{1ik}$, n_o – the water refractive index, R – the PMT rotation radius, x_k – the distance of particle k from the cuvette back wall, θ_i – the PMT rotation angle, θ_{1ik} – the angle of light scattering on a particle k incident after refraction on the back wall of the cuvette onto the centre of the PMT rotated by the angle θ_i.

Similarly, a dependence of the angle θ_{2ik} on θ_i for the scattering incident on the PMT after refraction on the cuvette side wall can be described. For both equations, the solution using the Cardano formulae for the fourth-degree equation can be found.

However, in order to more easily calculate the power of light scattered at angle θ_{1ik} measured by the PMT rotated at angle θ_i, the theoretical PMT rotation angle θ_{0ik} for this scattering angle (θ_{1ik}) was found assuming the absence of refraction from the quadratic equation

$$R^2\cos^2\theta_{0ik} - 2R(z_k - z_a)(1 - \cos^2\theta_{1ik})\cos\theta_{0ik}$$
$$+ (z_k - z_a)^2 (1 - \cos^2\theta_{1ik}) - R^2\cos^2\theta_{1ik} = 0, \qquad (7)$$

where z_a – the position of the PMT centre of rotation on the axis z, z_k – the position of particle k on the axis z.

2.4. Calculation of the kernel function $K(\theta_i, r_j)$

Since Mie formulae describe the scattered field in the spherical coordinate system of the scattering particle $(\theta_{1ik}, \varphi_{1ik})$, these formulae need to be transformed to the spherical coordinate system of the PMT rotation centre and rotated by the theoretical angle θ_{0ik}. Then, the power of the scattered light $P_{s\,ijk}$ from the particle z_k of the radius r_j

measured by the PMT located at angle θ_{0ik} to the direction of incident light $+z$, at a distance R from the axis of rotation is (2)

$$P_{s\,ijk} = \frac{I_p}{k_1^2} \int_0^{2\pi} \int_0^{\arctan\frac{r_0}{R}} \left[\begin{array}{l} |S_1(\cos\theta_{1ik}, r_j)|^2 \sin^2\varphi_{1ik} \\ + |S_2(\cos\theta_{1ik}, r_j)|^2 \cos^2\varphi_{1ik} \end{array} \right] \qquad (8)$$
$$\cdot \sin\theta_2 d\theta_2 d\varphi_2,$$

where

$$\cos\theta_{1ik}$$
$$= \frac{R(\cos\theta_2\cos\theta_{0ik} - \cos\varphi_2\sin\theta_2\sin\theta_{0ik}) + z_a - z_k}{\sqrt{R^2 + 2R(z_a - z_k)(\cos\theta_2\cos\theta_{0ik} - \cos\varphi_2\sin\theta_2\sin\theta_{0ik}) + (z_a - z_k)^2}}$$

$$\varphi_{1ik} = \arctan\frac{\sin\varphi_2\sin\theta_2}{\cos\theta_2\sin\theta_{0ik} + \cos\varphi_2\sin\theta_2\cos\theta_{0ik}}$$

r_0 – the radius of the PMT lens aperture.

Summing by the number of N particles located on the axis z inside the cuvette, we obtain the following equation:

$$K(\theta_i, r_j) = \sum_{k=1}^{N} P_{s\,ijk} . \qquad (9)$$

3. Experiment

In order to measure an angular distribution of the scattered light power, a laboratory angular scatterometer built at IOE [18] and shown schematically in Fig. 3 was used. A linearly polarised (parallel) laser beam L (He-Ne, Meredith Instruments) passes successively through a quartz flat-parallel plate (PP), a diaphragm (D), and through the centre of a horizontal cross section of a quartz cuvette C (Hellma GmbH) with a square base, containing a suspension of spherical polystyrene (PS) particles in water. Power of the incident beam on cuvette is P_o =7 mW.

Distance between opposite walls inside the cuvette is L = 10 mm, wall thickness equals 1 mm. To measure the scattered light power P_s, a PMT (H-5784 Hamamatsu) placed on a rotating arm at a distance R = 490 mm from the centre of rotation, coinciding with the centre of the cuvette cross-section was used. Both the cuvette and PMT were attached to a rotating table and a rotating arm, respectively, using precision adjustment table systems allowing the scatterometer to be adjusted. The rotation accuracy of the stepper motor-turned (SM) (Nanotec) table is 0.01°. The power of light incident on the cuvette was obtained by measuring the power of the reference beam P_r
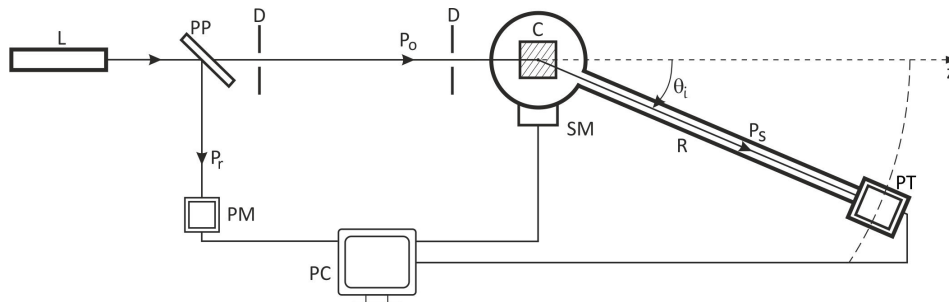

Fig. 3. Schematic of a laboratory angle scatterometer.

on a laser power meter (PM) (LaserMateQ Coherent). The program that controls the automatic operation of the laboratory scatterometer (in Matlab) uses an NI6014 data acquisition card (National Instruments). For the study, uncertified two initial samples (CV < 5%) containing by weight 10% spherical PS particles in aqueous suspension with mean radius and standard deviations were used respectively: 0.685 μm and 0.020 μm (PS-R-L2614), as well as 1.605 μm and 0.035 μm (PS-R-B1270-2) by Microparticles GmbH. From these initial samples, after an appropriate dilution (to avoid the significant effect of multiple scattering [19]), test samples were prepared with volume concentrations of about $1·10^{-4}$% and about $9.6·10^{-4}$%, respectively.

A mixture sample of the above materials was also prepared. After diluting the initial samples, particle volume concentrations were obtained for the mixture, respectively: $2.4·10^{-4}$% and $6.4·10^{-4}$% also allowing to avoid the effect of multiple dispersion.

The method of preparing the samples for the measurement was the following: the company container with particles was first subjected to gentle stirring with a magnetic stirrer, and then placed in an ultrasonic bath for several minutes to distribute the container particles evenly in the water. Then, a certain amount of the suspension thus prepared from the company container was added to the appropriate amount of the filtered water (to eliminate any scatterers other than the PS spheres) to obtain the desired concentration. The new sample thus obtained was gently re-stirred and then placed in an ultrasonic bath for several minutes to distribute the particles evenly in the water and remove air bubbles. The suspension thus prepared was gently placed in a clean quartz cuvette, the sides of which were additionally cleaned with spirit (denatured with ether).

Scattered light power measurements were conducted in a darkened room for the range of angles θ_i: from 7° to 41° every 1° from direction of the incidence of the laser beam ($+z$). Before the actual angular scattering measurements from the prepared samples, a background measurement – an angular measurement of the light scattering power from a cuvette filled with water was performed. The background measurement data were subtracted from the measurement data of the samples. The results of the measurements are shown in Figs. 4–6.

Since the samples tested were not certified, comparative measurements were made using a nanoDS instrument (CILAS). The following results (mean radius, standard deviation) were obtained:

- for the sample PS-R-L2614: (0.676 μm, 0.031 μm)
- for the sample PS-R-B1270-2: (1.573 μm, 0.041 μm).

4. Calculations

The following data were used for the calculations:

- wavelength of the laser light (in vacuum): $\lambda = 0.6328$ μm,
- refractive index of the medium (H$_2$O) [20]: $n_o = 1.3317$,
- refractive index of the particle material [21]: $n_r = 1.5824+0.0005I$,
- power of the laser beam incident on the particles: $P_p = 6.84$ mW,
- distance of the rotation centre from the Gaussian beam waist: $z_a = 1057$ mm,

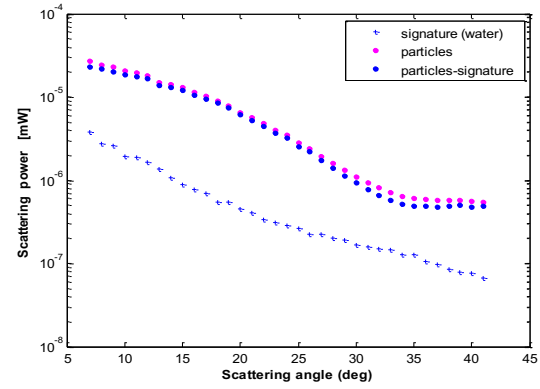**Fig. 4.** Measurement of scattering power and background as a function of the scattering angle for particles with a radius of 0.676 μm.

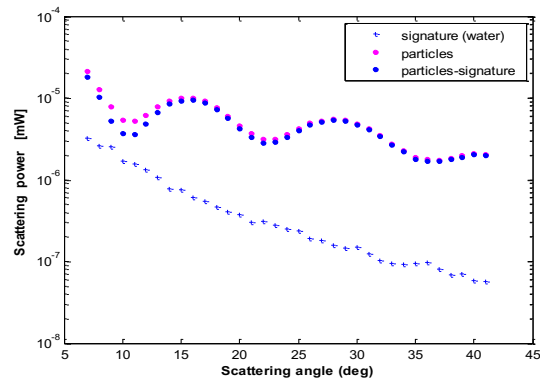**Fig . 5.** Measurement of scattering power and background as a function of the scattering angle for particles with a radius of 1.573 μm.
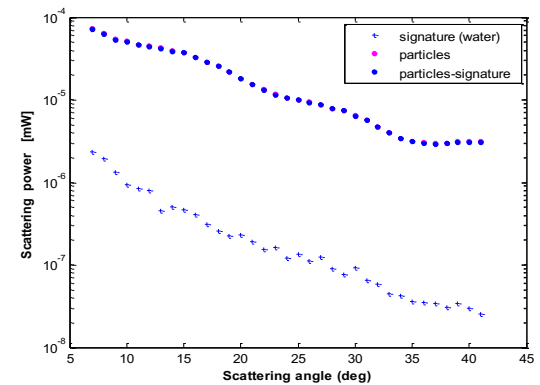

Fig. 6. Measurement of scattering power and background as a function of the scattering angle for a mixture of particles.

- radius of the Gaussian beam at the beam waist: $w_0 = 0.4$ mm,
- distance of the PMT lens aperture from the rotation centre: $R = 490$ mm,
- radius of the PMT lens aperture: $r_0 = 1.5$ mm,
- radius of the Gaussian beam for $z = z_a$: $w(z_a) = 0.6659$ mm.

The model of a series of equidistant particles located on the z-axis inside the cuvette symmetrically to the centre of rotation was adapted. It was assumed that the laser beam illuminating this series of particles is a plane wave with the constant intensity I_p equal to the intensity of the beam for the centre of rotation. For the above data

$$I_p = \frac{2P_p}{\pi w(z_a)^2} = 9820 \frac{\text{W}}{\text{cm}^2} .$$

For the calculation of the function $K(\theta_i, r_j)$, the values of the angle θ_i were assumed to be the same as the adopted values of the PMT rotation angle when measuring the power of scattered light (identical for three suspensions of microparticles tested), that is: $\theta_1 = 7°$ every $\Delta\theta = 1°$ to $\theta_{35} = 41°$. The values of the radius r_j were adopted depending on the size of the tested microparticles:

- for particles with a radius of 0.685 µm: $r_1 = 0.220$ µm every $\Delta r = 0.040$ µm to $r_{35} = 1.580$ µm,
- for particles with a radius of 1.605 µm: $r_1 = 0.730$ µm every $\Delta r = 0.060$ µm to $r_{35} = 2.770$ µm,
- for mixture of the above particles: $r_1 = 0.385$ µm every $\Delta r = 0.070$ µm to $r_{35} = 2.765$ µm.

Preliminary calculations were carried out for a single scattering particle located on the rotation axis, and for 10 and 20 particles evenly distributed on the z-axis inside the cuvette. For each particle, the power of the scattered light given by the PMT was separately counted as a function of the angle θ_i and the radius r_j, and then the powers from individual scatterers were summed. It turned out that for a given measurement geometry (Fig. 2), for a detection angle $\theta_i \in (7°, 41°)$, the effect of the scattered light refracted on the side wall of the cuvette and the effect of the transmission of the scattered light on the amount of power given by the PMT is negligible. In addition, it was found out that by solving the inverse problem (with the modified Twomey method) for the 10-particle and 20-particle model and then applying the Levenberg-Marquardt approximation to the Gaussian function for the calculated solutions, the same parameters of the distributions were obtained. And also that there are small differences in these parameters for the 1-particle model in the rotation axis. Therefore, a model of 10 particles equidistant from each other inside the cuvette was adopted.

4.1. Solution by the first way using the Tikhonov method

Equation (3) can be written in matrix form

$$\boldsymbol{P_s} = \boldsymbol{K1}\boldsymbol{n_v}, \tag{10}$$

then the solution obtained by the Tikhonov method is given by the formula [1, 2]

$$\boldsymbol{n_v} = (\boldsymbol{K1}^T\boldsymbol{K1} + \alpha_1\boldsymbol{I})^{-1}\boldsymbol{K1}^T\boldsymbol{P_s}, \tag{11}$$

where: $\boldsymbol{I}$ – the unit matrix, α_1 – the regularization parameter obtained from L-curve criterion [15–17].

L-curve is a set of points $(\log\|\boldsymbol{K1}\boldsymbol{n_v^{\alpha_1}} - \boldsymbol{P_s}\|_2$, $\log\|\boldsymbol{n_v^{\alpha_1}}\|_2)$ depending on α_1, $\|\boldsymbol{n_v^{\alpha_1}}\|_2$ – the solution norm for the parameter α_1, $\|\boldsymbol{K1}\boldsymbol{n_v^{\alpha_1}} - \boldsymbol{P_s}\|_2$ – the residual norm for α_1. The L-curve criterion is as follows: the optimal regularization parameter α_{1opt} corresponds to the point of the L-curve with the maximum curvature.

To improve the solution obtained by the Tikhonov method for narrow distributions (for these distributions,

there is a significant over-smoothing of the obtained results), equation (10) was modified by scaling it with the diagonal matrix N_v for the solution n_v obtained from (11) for this formula. Then,

$$\boldsymbol{P_s} = (\boldsymbol{K1}\ \boldsymbol{N_v})(\boldsymbol{N_v^{-1}}\ \boldsymbol{n_v}) = \boldsymbol{K2}\boldsymbol{n_{v1}}, \tag{12}$$

where

$$\boldsymbol{K2} = \boldsymbol{K1}\boldsymbol{N_v}, \quad \boldsymbol{n_{v1}} = \boldsymbol{N_v^{-1}}\boldsymbol{n_v}, \quad \boldsymbol{N_v} = diag(\boldsymbol{n_v}).$$

For the new equation (12), the solution by the Tikhonov method is found

$$\boldsymbol{n_{v1}} = (\boldsymbol{K2}^T\boldsymbol{K2} + \alpha_2\boldsymbol{I})^{-1}\boldsymbol{K2}^T\ \boldsymbol{P_s}. \tag{13}$$

Then, we find the parameter α_2 from the new L curve for (12) and finally

$$\boldsymbol{n_v} = \boldsymbol{N_v}\boldsymbol{n_{v1}}. \tag{14}$$

The solution $\boldsymbol{n_v}$ applies to both single particle distributions and their sum. To approximate the solution $\boldsymbol{n_v}$ to a Gaussian distribution, the Gaussian function f_g was fitted using the Levenberg-Marquardt method [8, 9] to solutions for single particle distributions and, accordingly, the bimodal Gaussian function f_{bg} for their sum. We can write the functions f_g and f_{bg} in the form

$$f_g = \frac{a}{\sigma\sqrt{2\pi}}e^{\frac{-(r-\bar{r})^2}{2\sigma^2}} = (a, \bar{r}, \sigma),$$

$$f_{bg} = \frac{a_1}{\sigma_1\sqrt{2\pi}}e^{\frac{-(r-\overline{r_1})^2}{2\sigma_1^2}} + \frac{a_2}{\sigma_2\sqrt{2\pi}}e^{\frac{-(r-\overline{r_2})^2}{2\sigma_2^2}}$$
$$= (a_1, \overline{r_1}, \sigma_1, a_2, \overline{r_2}, \sigma_2) .$$

4.2. Solution by the second way using the modified Twomey method

Equation (3) can be written in a simplified form as

$$P_s(i) = \sum_{j=1}^{n} K1(i,j)\, n_v(j), \quad i = 1 \dots n. \tag{15}$$

An initial constant value of the distribution sought: $n_v^0(j) = [1, 1, 1, \dots 1]$, and the number of iterations: l can be assumed. The solution by the modified Twomey method is given as a successive iterative approximation of the function $n_v^l(j)$ calculated from the formula [3, 4]

$$n_v^l(j) = n_v^{l-1}(j) \prod_{i=1}^{n}\left\{1 + \frac{2[a^{l-1}(i) - 1]K2(i,j)}{M_a(j)}\right\}, \tag{16}$$
$$i, j = 1 \dots n$$

where

$$a^{l-1}(i) = \frac{P_s(i)}{\max[K1(i)]\, P_{sc}^{l-1}(i)},$$

$$P_{sc}^{l-1}(i) = \sum_{j=1}^{n} K2(i,j)n_v^{l-1}(j),$$

$$K2(i) = \frac{K1(i)}{\max[K1(i)]},$$

$$M_a(j) = \sum_{i=1}^{n} K2(i,j).$$

Initial solutions for the densities of the volume distributions n_v were obtained for the number of iterations $l = 90$, both for the individual narrow distributions and for their sum. Fitting was then performed with the Gaussian function f_g and the bimodal Gaussian function f_{bg} using the Levenberg-Marquardt method to the corresponding solutions.

It turned out, compared with the results obtained with nanoDS, that these solutions determine the average radii for individual distributions quite well and a bit worse for their sum (like the Tikhonov method). However, to reduce the occurring broadening of the distributions (less than in the Tikhonov method), additional calculations were introduced into the calculation algorithms to better approximate the distribution width parameter.

4.2.1　Singular narrow distributions

For the singular narrow distributions, an optimisation was made of the n_v^l distributions calculated for each iteration l with respect to measured data. To this end, an additional parameter sigma(l) was calculated for an assumed sufficiently large number of iterations l, and it was then determined for which value $l = l_{opt}$ the parameter sigma (l) reaches the minimum.

$$\text{sigma}(l)$$
$$= \sqrt{\frac{1}{n}\sum_{i=1}^{n}\left[\left(\frac{s_1(i,l)}{\max(s_1)} - \frac{P_s(i)}{\max(P_s)}\right)\bigg/\frac{P_s(i)}{\max(P_s)}\right]^2}, \quad (17)$$

where

$$s_1(i,l) = \sum_{j=1}^{n} K1(i,j)n_v^l(j).$$

For the distribution $n_v^{l_{opt}}$ thus obtained, after fitting with the Gaussian function (Levenberg-Marquardt method), the parameters $(a, \bar{r}, \sigma)$ of the distribution were obtained.

4.2.2　Sum of two narrow distributions

For the sum of two single narrow distributions, a different method was used. The values $\bar{r}_1$ and $\bar{r}_2$ obtained from the bimodal Gaussian fit for $l = 90$ were assumed to be correct (the difference between them and the values obtained for the single distributions is about 1%). In order to determine more precisely the width of the first distribution σ_1, the appropriately normalised data

$$s_2(i) = \sum_{j=1}^{n} K1(i,j)\frac{a_2}{\sigma_2\sqrt{2\pi}}e^{\frac{-(r_j-\bar{r}_2)^2}{2\sigma_2^2}}$$

corresponding to the less broadened second distribution were first subtracted from the measured data P_s.

For the new data thus obtained, a new single first distribution (for $l = 90$) was calculated, and a Gaussian function was fitted to it. Hence, the corrected width of the first distribution (σ_1) was obtained. In an analogous manner, the new corrected width of the second distribution was calculated by subtracting the appropriately normalised data corresponding to the new corrected first distribution from the measured data. Next, optimisation of the height of the new bimodal Gaussian first peak (with new peak widths) was performed against the measured data by taking the parameter a_1 of the bimodal Gaussian as a variable and calculating for which value of a_1 the expression below reaches the minimum

$$\sqrt{\frac{1}{n}\sum_{i=1}^{n}\left[\left(\frac{d(i,a_1)}{\max(d)} - \frac{P_s(i)}{\max(P_s)}\right)\bigg/\frac{P_s(i)}{\max(P_s)}\right]^2}, \quad (18)$$

where

$$d(i,a_1) = \sum_{j=1}^{n} K1(i,j)f_{bg}(j,a_1).$$

4.3.　Calculations results

As a result of the calculations, the frequency curve $q3(r_j)$ and the cumulative curve $Q3(r_j)$ were obtained for a volume-weighted distribution [22]

$$q3(r_j) = \frac{n_v(r_j)}{\sum_{j=1}^{n} n_v(r_j)}, \quad (19)$$

$$Q3(r_k) = \sum_{j=1}^{k} q3(r_j)\Delta r.$$

Figures 7 and 8 present the first distribution obtained by the Tikhonov method and by the first way using Tikhonov method. Second distribution obtained by analogy is shown in Figs. 9 and 10.

In the Tikhonov method, for both single particle distributions, the solutions obtained in the form of Gaussian distributions have the positions of both maxima $\bar{r}$ close to the corresponding values obtained with nanoDS, while the widths of these distributions σ are three times and two times higher than the corresponding results obtained with nanoDS (Figs. 7, 9). After rescaling the obtained solutions of the initial equations and then solving the new equations using the Tikhonov method, new solutions were obtained in the form of Gaussian distributions with much smaller widths and small changes in the positions of the maxima (Figs. 8, 10) compared to the results obtained for the unscaled equations.

Sum of two distributions obtained by the Tikhonov method and by the first way using the Tikhonov method is presented in Figs. 11 and 12.

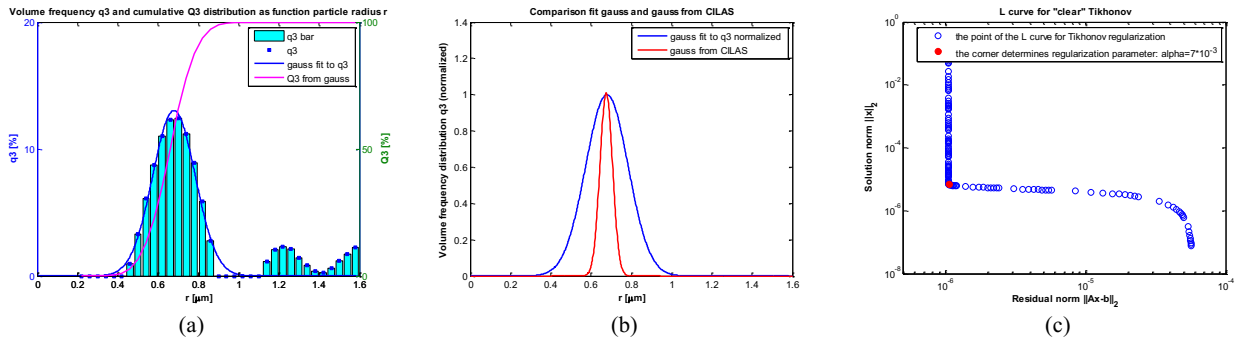**First distribution obtained by the Tikhonov method**
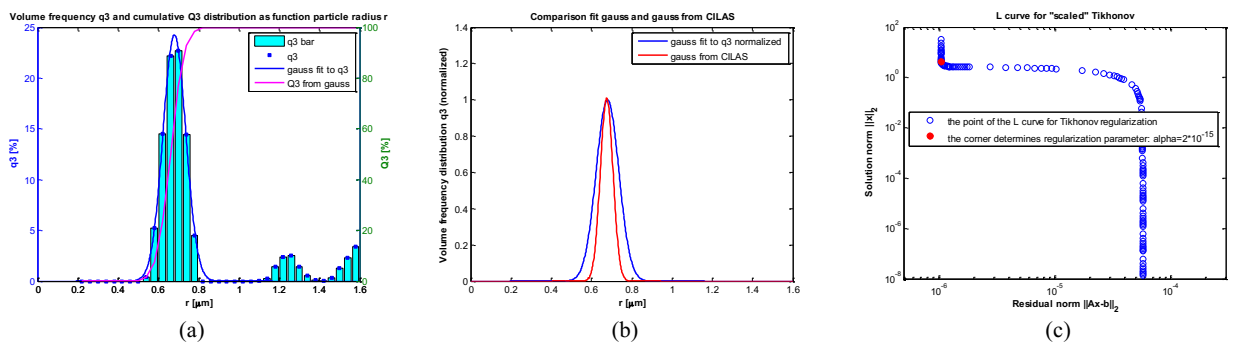

(a)	(b)	(c)

Fig. 7. (a) Gaussian fit to the $q3$ calculations result obtained by the Tikhonov method. Parameters obtained: (a, $\bar{r}$, σ) = (0.00003448, 0.679 µm, 0.105 µm). (b) Comparison with Gauss obtained from measurements with nanoDS: (a, $\bar{r}$, σ) = (0.00007917, 0.676 µm, 0.031 µm). (c) L-curve and regularisation parameter α.

First distribution obtained by the first way using Tikhonov method

(a)	(b)	(c)

Fig. 8. (a) Gaussian fit to the $q3$ calculations result obtained by the first way using Tikhonov method. Parameters obtained: (a, $\bar{r}$, σ) = (0.00003432, 0.680 µm, 0.057 µm). (b) Comparison with Gauss obtained from measurements with nanoDS. (c) L-curve and regularisation parameter α.
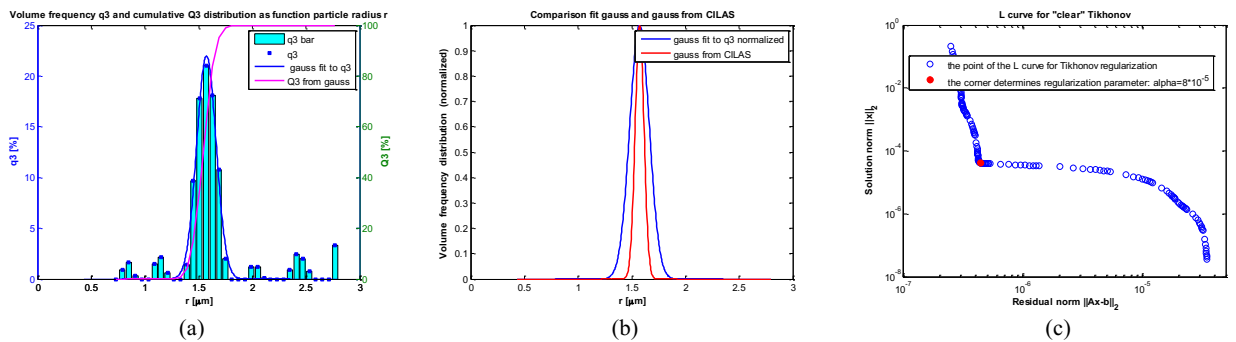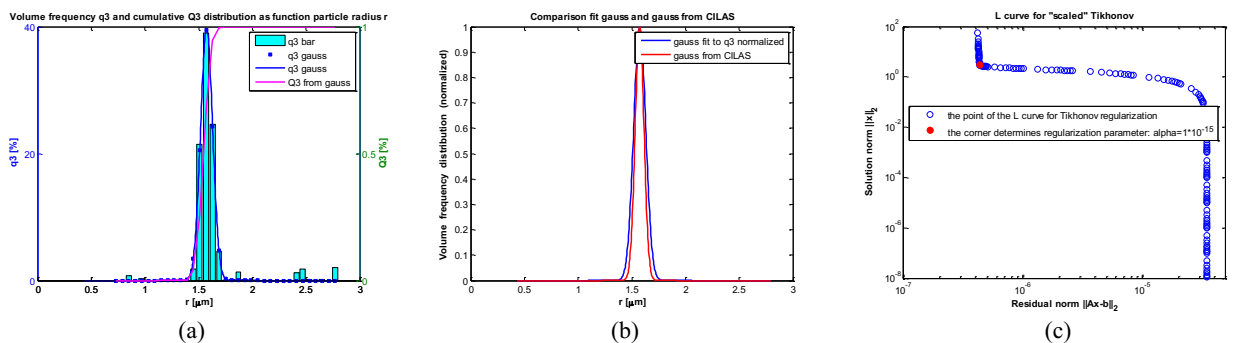
Second distribution obtained by the Tikhonov method

(a)	(b)	(c)

Fig. 9. (a) Gaussian fit to the $q3$ calculations result obtained by the Tikhonov method. Parameters obtained: (a, $\bar{r}$, σ) = (0.00004998, 1.573 µm, 0.091 µm). (b) Comparison with Gauss obtained from measurements with nanoDS: (a, $\bar{r}$, σ) = (0.0001028, 1.573 µm, 0.041 µm). (c) L-curve and regularisation parameter α.

Second distribution obtained by the first way using Tikhonov method:

(a)	(b)	(c)

Fig. 10. (a) Gaussian fit to the $q3$ calculations result obtained by the first way using Tikhonov method. Parameters obtained: (a, $\bar{r}$, σ) = (0.00005580, 1.574 µm, 0.056 µm). (b) Comparison with Gauss obtained from measurements with nanoDS. (c) L-curve and regularisation parameter α.

For the sum of two single particle distributions, a significantly broadened bimodal Gaussian distribution (more broadened first peak) and small shifts in the positions of the maxima of both peaks ($\bar{r}_1, \bar{r}_2$) towards larger values were obtained using the Tikhonov method compared to the results obtained for the single distributions obtained with nanoDS (Fig. 11). For the scaled equation, the computational results show a significant reduction in the width of both Gaussian peaks and small changes in the positions of the maxima of both peaks (Fig. 12) compared to the results obtained for the unscaled equation.

Figures 13 and 14 present respectively the first and the second distributions obtained by the modified Twomey method with an optimal number of iterations. In this method, for both individual particle size distributions, the obtained

solutions in the form of Gaussian distributions have positions of both maxima ($\bar{r}$) and widths of the distributions (σ) close to the corresponding values obtained with nanoDS.

For the sum of two single particle size distributions, for number of iterations $l = 90$, a broadened bimodal Gaussian distribution (much broadened first peak, little broadened second peak) and a shift towards larger values at the positions of the maxima of both peaks ($\bar{r}_1, \bar{r}_2$) compared to the results of the single distributions obtained with nanoDS were obtained. Using the method of a subsequent subtraction of the data corresponding to the single peaks from the measured data and optimisation of the height of the first peak, the widths of both distributions were obtained close to the corresponding values obtained from the nanoDS (Fig. 15).

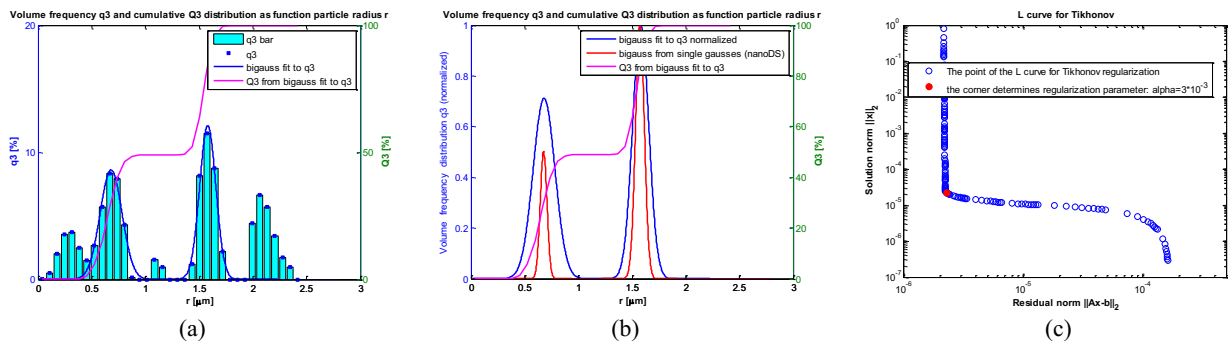**Sum of two distributions obtained by the Tikhonov method**

Fig. 11. (a) Bimodal Gaussian fit to the $q3$ calculations result obtained by the Tikhonov method. The parameters obtained: $(a_1, \bar{r}_1, \sigma_1, a_2, \bar{r}_2, \sigma_2) = (0.00002198, 0.680~\mu m, 0.102~\mu m, 0.00002290, 1.580~\mu m, 0.076~\mu m)$. (b) Comparison with bimodal Gauss obtained from single distribution measurements with nanoDS. (c) L-curve and regularisation parameter α.

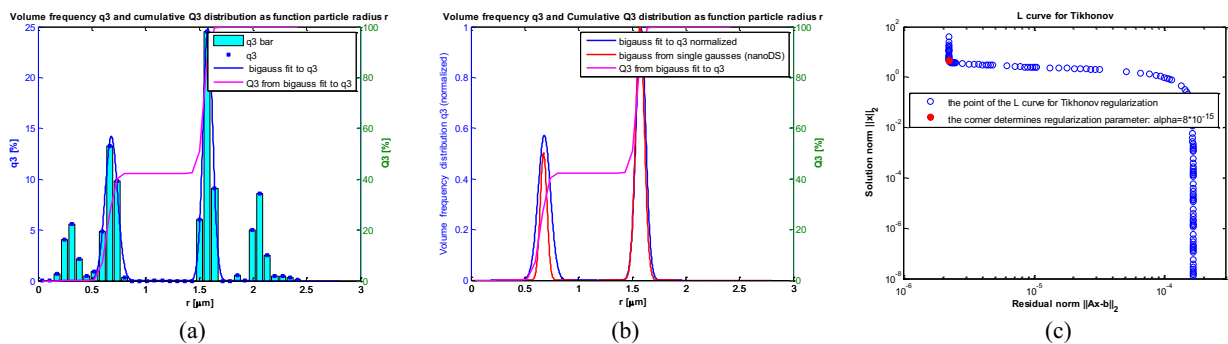**Sum of two distributions obtained by the first way using the Tikhonov method**

Fig. 12. (a) Bimodal Gaussian fit to the $q3$ calculations result obtained by the first way using Tikhonov method. The parameters obtained: $(a_1, \bar{r}_1, \sigma_1, a_2, \bar{r}_2, \sigma_2) = (0.00002061, 0.682~\mu m, 0.058~\mu m, 0.00002805, 1.581~\mu m, 0.045~\mu m)$. (b) Comparison with bimodal Gauss obtained from single distribution measurements with nanoDS. (c) L-curve and regularisation parameter α.

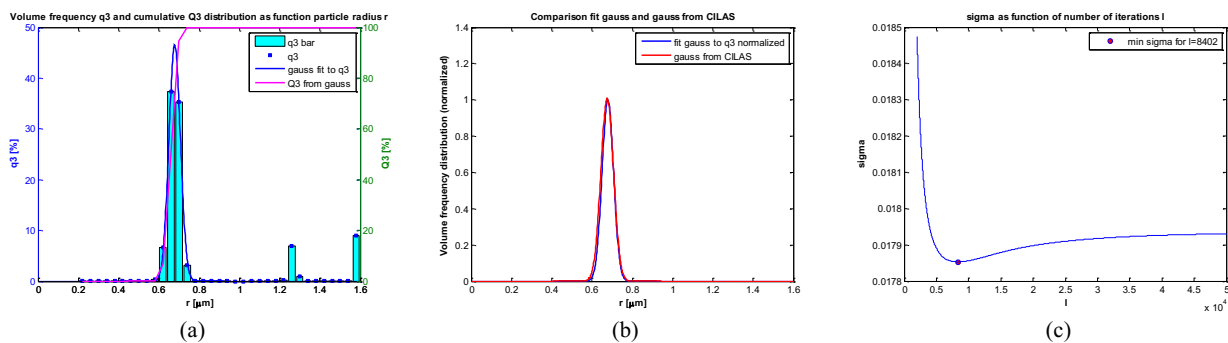**First distribution obtained by the modified Twomey method with an optimal number of iterations**

Fig. 13. (a) Gaussian fit to the $q3$ calculations result obtained by the modified Twomey method. The parameters obtained: $(a, \bar{r}, \sigma) = (0.00003317, 0.678~\mu m, 0.029~\mu m)$. (b) Comparison with Gauss obtained from measurements with nanoDS: $(a, \bar{r}, \sigma) = (0.00007917, 0.676~\mu m, 0.031~\mu m)$. (c) Optimal number of iterations $l_{opt} = 8402$ for sigma minimum.

Second distribution obtained by the modified Twomey method with an optimal number of iterations

(a)   (b)   (c)
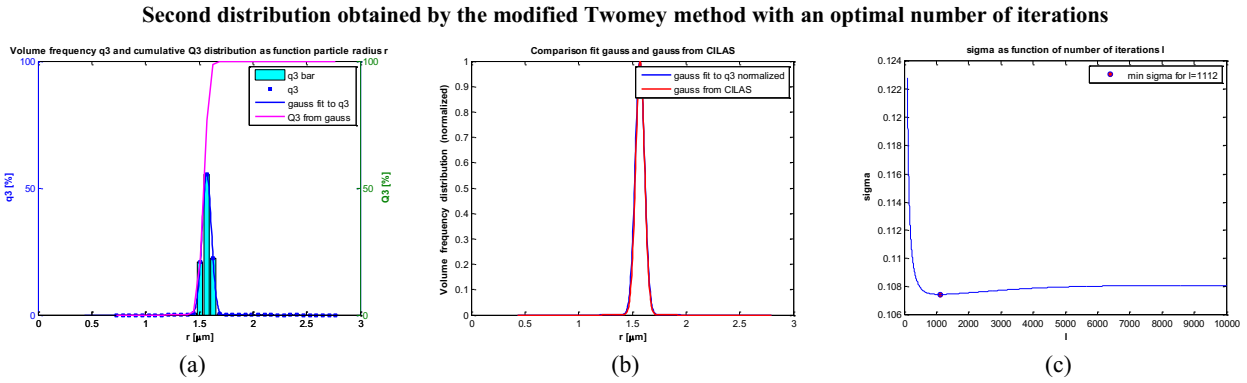
Fig. 14. (a) Gaussian fit to the $q3$ calculations result obtained by the modified Twomey method. The parameters obtained: $(a, \bar{r}, \sigma) = (0.00006059, 1.571\ \mu m, 0.044\ \mu m)$. (b) Comparison with Gauss obtained from measurements with nanoDS: $(a, \bar{r}, \sigma) = (0.0001028, 1.573\ \mu m, 0.041\ \mu m)$. (c) Optimal number of iterations $l_{opt} = 1112$ for sigma minimum.

Sum of two distributions obtained by the second way using the modified Twomey method

(a)   (b)
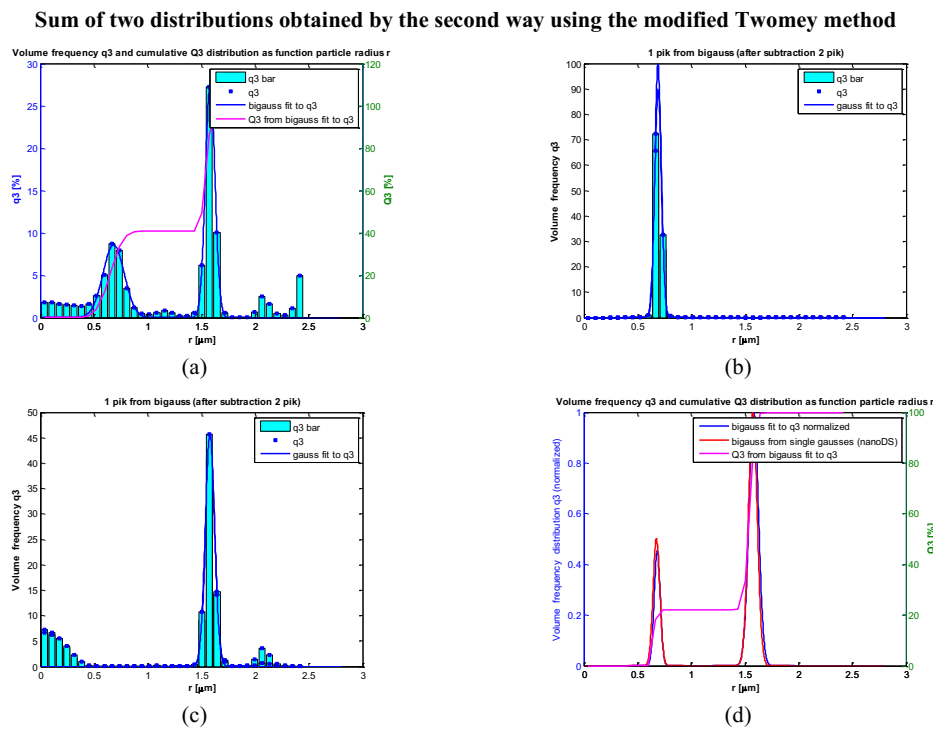
(c)   (d)

Fig. 15. (a) Bimodal Gaussian fit to the $q3$ calculations result obtained by the second way using the modified Twomey method (for number of iterations $l = 90$). The parameters obtained: $(a_1, \bar{r}_1, \sigma_1, a_2, \bar{r}_2, \sigma_2) = (0.00002132, 0.683\ \mu m, 0.099\ \mu m, 0.00003081, 1.582\ \mu m, 0.045\ \mu m)$. (b) Peak 1 $(\sigma_1 = 0.032\ \mu m)$ obtained for $l = 90$ after subtracting the data corresponding to peak 2. (c) Peak 2 $(\sigma_2 = 0.043\ \mu m)$ obtained for $l = 90$ after subtracting the data corresponding to the new peak 1. (d) Bimodal Gaussian parameters with new widths (σ_1, σ_2) of the peaks and after optimisation of the parameter a_1 of peak 1: $(a_1, \bar{r}_1, \sigma_1, a_2, \bar{r}_2, \sigma_2) = (0.00000881, 0.683\ \mu m, 0.032\ \mu m, 0.00003081, 1.582\ \mu m, 0.043\ \mu m)$. Comparison with bimodal Gaussian obtained from single distribution measurements with nanoDS.

5.   Conclusions

For the narrow particle size distributions under study (CV < 5%), the Tikhonov method allows for a fairly good determination of the positions of the maxima for single distributions and somewhat worse one for their sum. The large broadening (even several times) of the widths of the tested distributions occurring in this method, as compared to their actual widths (both in single distributions and their sum) with nanoDS was significantly reduced (by about 40–50%) by calculating a new distribution for the initial equation scaled by the distribution obtained for this equation (the first way using the Tikhonov method).

The modified Twomey method, thanks to the estimation of the optimal number of iterations, allows not only for a fairly good determination of the positions of the maxima (as in the Tikhonov method), but also of the widths of the narrow singular distributions under study. For the sum of two narrow distributions, for a number of iterations of $l = 90$, the positions of both maxima were obtained close to the values obtained by the Tikhonov method. The application of the method of successive subtraction of the data corresponding to the calculated singular distributions from the measured data and optimisation of the height of the first distribution (the second way using the modified Twomey method) made it possible to determine the widths of both distributions quite well, better than for the Tikhonov method.

Acknowledgements

References

[1] Tikhonov, A. N., Goncharsky, A. V., Stepanov, V. V. & Yagola, A. G. *Numerical Methods for The Solution of Ill-Posed Problems.* (Kluwer Academic Publishers, Dordrecht 1995).

[2] Groetsch, C. W. *The Theory of Tikhonov Regularization for Fredholm Equations of The First Kind.* (Boston-London-New York, Pitman Publishing 1984).

[3] Igushi, T. & Yoshida, H. Investigation of low-angle laser light scattering patterns using the modified twomey iterative method for particle sizing. *Rev. Sci. Instrum.* **82**, 015111 (2011). https://doi.org/10.1063/1.3520136

[4] Igushi, T. & Yoshida, H. Influence of the number of detectors by laser scattering method for estimation of particle size. *Rev. Sci. Instrum.* **83**, 055103 (2012). https://doi.org/10.1063/1.4709493

[5] Twomey, S. Comparison of constrained linear inversion and an iterative nonlinear algorithm applied to the indirect estimation of particle size distributions. *J. Comput. Phys.* **18**, 188–200 (1975). https://doi.org/10.1016/0021-9991(75)90028-5

[6] Twomey, S., Herman, B. & Rabinoff, R. An extension to the Chahine method of inverting the radiative transfer equation. *J. Atmos. Sci.* **34**, 1085–1090 (1977). https://doi.org/10.1175/1520-0469(1977)034<1085:AETTCM>2.0.CO;2

[7] Markowski, G. R. Improving Twomey's algorithm for inversion of aerosol measurement data. *Aerosol Sci. Technol.* **7**, 127–141 (1987). https://doi.org/10.1080/02786828708959153

[8] Marquardt, D. W. An algorithm for least-squares estimation of nonlinear parameters. *J. Soc. Ind. Appl. Math.* **11**, 431–441 (1963). https://doi.org/10.1137/0111030

[9] Madsen, K., Nielsen, H. B. & Tingleff, O. *Methods for Non-Linear Least Squares Problems 2nd edition* (Technical University of Denmark, 2004). http://www2.imm.dtu.dk/pubdb/edoc/imm3215.pdf

[10] Weiner, I., Rust, M. & Donelly, T. D. Particle size determination: an undergraduate lab in Mie scattering. *Am. J. Phys.* **69**, 129–136 (2001). https://doi.org/10.1119/1.1311785

[11] van de Hulst, H. C. *Light Scattering by Small Particles.* (Dover Publications, New York, 1981).

[12] Bohren, C. F. & Huffman, D. R. *Absorption and Scattering of Light by Small Particles.* (Wiley, New York, 1983).

[13] Kandlikar, M. & Ramachandran, G. Inverse methods for analysing aerosol spectrometer measurements: A critical review. *J. Aerosol Sci.* **30**, 413–437 (1998). https://doi.org/10.1016/S0021-8502(98)00066-4

[14] Wiscombe, W. *Mie Scattering Calculations: Advances in Technique and Fast Vector-Speed Computer Code.* (NCAR, 1996).

[15] Hansen, P. C. *The L-Curve and its Use in The Numerical Treatment of Inverse Problems* (Technical University of Denmark, 2000).

[16] Hansen, P. C., Jensen, T. K. & Rodriguez, G. An adaptive pruning algorithm for the discrete l-curve criterion. *J. Comput. Appl. Math.* **198**, 483–492 (2005). https://doi.org/10.1016/j.cam.2005.09.026

[17] Castellanos, J. L., Gomez, S. & Guerra, V. The triangle method for finding the corner of the L-curve. *Appl. Numer. Math.* **43**, 359–373 (2002). https://doi.org/10.1016/S0168-9274(01)00179-9

[18] Pawlata, A. Examination of smooth surfaces roughness using angle scatterometer, part.1. The method of measurement. The measurement instrument. *Bulletin of Military University of Technology* **64**, 47–58 (2015). https://doi.org/10.5604/12345865.1145426

[19] Particle size analysis – Laser diffraction methods. *ISO 13320* (2009). https://www.iso.org/standard/44929.html

[20] Hale, G. M. & Querry, M. R. Optical constants of water in the 200nm to 200μm wavelength region. *Appl. Opt.* **12**, 555–563 (1973). https://doi.org/10.1364/AO.12.000555

[21] Ma, X. *et al*. Determination of complex refractive index of polystyrene microspheres from 370 to 1610 nm. *Phys. Med. Biol.* **48**, 4165–4172 (2003). https://doi.org/10.1088/0031-9155/48/24/013

[22] Xu, R. *Particle Characterization.* (Kluwer Academic Publishers, Dordrecht, 2000)